Journal of Magnetic Resonance **137,** 258–264 (1999)
Article ID jmre.1998.1688, available online at http://www.idealibrary.com on IDEAL®

Xenon-131 Surface Sensitive Imaging of Aerogels in Liquid Xenon near the Critical Point

Galina Pavlovskaya,* Ashley K. Blue,* Stephen J. Gibbs,*,†,[1] Mathias Haake,‡
Frederic Cros,§ Laurent Malier,§ and Thomas Meersmann*,[1,2]

*Center for Interdisciplinary Magnetic Resonance, National High Magnetic Field Laboratory, 1800 East Paul Dirac Drive, Tallahassee, Florida 32310; †Department of Chemical Engineering, FAMU-FSU College of Engineering, Tallahassee, Florida 32306; ‡Department of Chemical Engineering, University of California at Berkeley, Berkeley, California 94720; and §Laboratoire de Physique de la Matière Condensée, CNRS, Ecole Polytechnique, 91128 Palaiseau Cedex, France

Received July 30, 1998; revised December 7, 1998

In recent years, optically pumped xenon-129 has received a great deal of attention as a contrast agent in gas-phase imaging. This report is about the other NMR active xenon isotope (i.e., xenon-131, $S = \frac{3}{2}$) which exhibits distinctive features for imaging applications in material sciences that are not obtainable from xenon-129 ($S = \frac{1}{2}$). The spin dynamics of xenon-131 in gas and liquid phases is largely determined by quadrupolar interactions which depend strongly on the surface of the surrounding materials. This leads to a surface dependent dispersion of relaxation rates, which can be substantial for this isotope. The dephasing of the coherence due to quadrupolar interactions may be used to yield surface specific contrast for imaging. Although optical pumping is not practical for this isotope because of its fast quadrupolar relaxation, a high spin density of liquid xenon close to the critical point (289 K) overcomes the sensitivity problems of xenon-131. We report the first xenon-131 magnetic resonance images and have tested this technique on various meso-porous aerogels as host structures. Aerogels of different densities and changing levels of hydration can clearly be distinguished from the images obtained.

Key Words: **xenon-131; surface sensitive imaging; quadrupolar relaxation; meso porous materials; aerogels.**

INTRODUCTION

Xenon nuclear magnetic resonance spectroscopy has been increasingly used during the past two decades as a non-invasive probe in chemistry and material sciences. The large electron cloud of the relatively inert xenon atom is highly polarizable, leading to a large chemical shift range, which makes it a sensitive probe for its environment (*1–6*) . For recent reviews, the reader is referred to the work of Raftery and Chmelka (*7*) and Ratcliffe (*8*). The majority of the previous xenon NMR research was focused on the isotope xenon-129 due to the larger magnetogyric ratio (27.81% of the proton Larmor frequency), and its higher natural abundance (26.44%) compared to the other isotope xenon-131 (8.25% of the proton Larmor frequency, 21.18% natural abundance). However, the xenon-131 isotope has a spin $S = \frac{3}{2}$ and thus a quadrupolar moment which can be exploited to provide valuable information not available from xenon-129 with its spin $I = \frac{1}{2}$. Therefore, xenon-131 has been used for studies concerning the nematic phase of thermotropic liquid crystalline solutions (*9–12*), was recently introduced as a tool for surface investigations using multiple quantum filtering (*13*), and has been applied to probe the distortion of the atomic electron density by the external magnetic field (*14*). In this report, the authors introduce the application of xenon-131 for obtaining unique contrast in magnetic resonance imaging (MRI) in material science. Alumino-silicate aerogels have been chosen as a test material for this technique. Previously, Gregory *et al.* studied similar aerogels using ^{129}Xe MRI and NMR (*15, 16*).

MRI of optically polarized gas phase helium-3 and xenon-129 either in gas phase or dissolved in liquids has gained increasing interest for medical applications (*17–20*). Optical pumping of xenon-129 provides sufficient signal intensities (*21*) for MRI, which are otherwise hard to obtain for gases under atmospheric pressure or at low concentrations. Unfortunately, optical pumping of xenon-131 is not feasible for most applications because of the fast quadrupolar relaxation of this isotope. However, the apparent disadvantage of quadrupolar relaxation can be turned into a benefit since it depends strongly on the surface properties of the materials surrounding the xenon-131, thus leading to a substantial dispersion of relaxation rates in different materials. This makes xenon-131 potentially useful for obtaining unique contrast in MRI of meso-porous materials.

EXPERIMENTAL

There are three factors that contribute to a sufficient signal intensity for the xenon-131 imaging experiments under discussion:

[1] To whom correspondence should be addressed. E-mail: meersman@dirac.cchem.berkeley.edu, gibbs@magnet.fsu.edu.

[2] Current address: Department of Chemistry, University of California at Berkeley, Berkeley, CA 94720.

1090-7807/99 $30.00

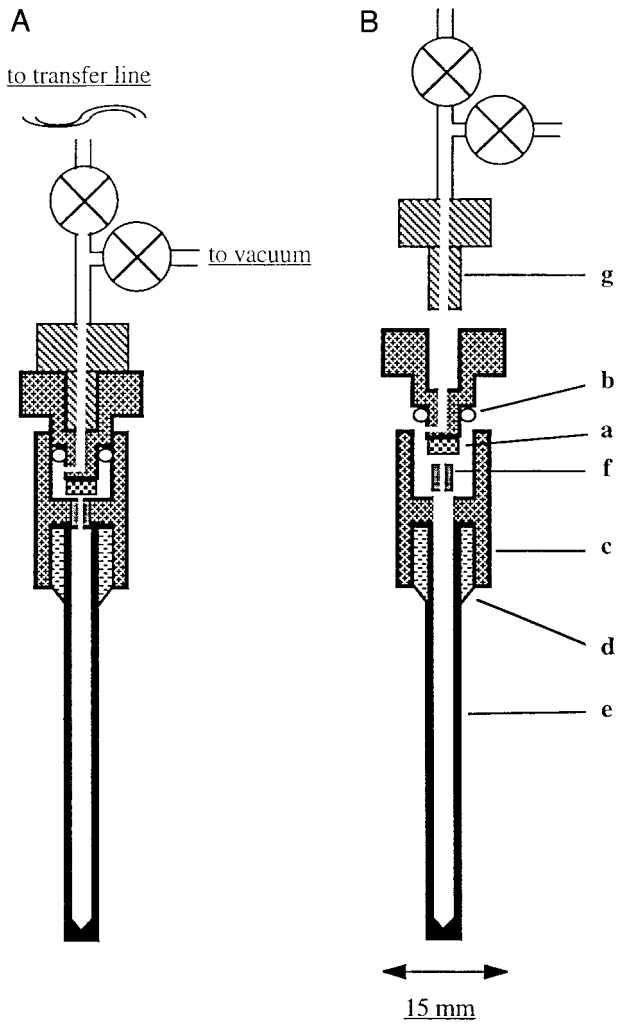

FIG. 1. (A) Sketch of the high pressure sapphire NMR tube and BeCu-alloy valve. The primary seal is open and the secondary seal is closed during the xenon filling procedure. (B) Exploded view of the tube. The primary seal (a) is made from Vespel, and the secondary seal (b) is a regular Viton-O-ring that holds the gas up to a pressure of ca. 7 MPa during the filling procedure. The valve system is glued with a special epoxy (Aremco568) (d) to the sapphire tube (e). An inlet screw (f) with a small capillary opening reduces the force on the primary seal, but it can be removed in order to transfer bulk material (i.e., the aerogel) into the tube. The system was connected to a stainless steel transfer line via swagelock fittings.

(1) The experiments were performed at very high fields (600 MHz for protons, i.e., 49 MHz for Xe-131);

(2) Liquid xenon close to the critical temperature (289 K) was used, thus providing a high spin density in addition to gas-like relaxation behavior;

(3) The short relaxation time of the xenon-131 in an aerogel ($T_1 \approx$ 3–11 ms depending on aerogel properties and experimental conditions) enables fast signal accumulation.

The significance of xenon-131 for obtaining unique contrast in various aerogels was tested. Recently, the first xenon-129 images were successfully recorded (*15*). Aerogels were first synthesized in the early 1930s by Kistler (*22*) and received widespread attention in the 1980s and 1990s because of their unique thermal, optical, and mechanical properties (*23, 24*). These unusual properties are determined by the structure of these materials in which the fragile solid network is preserved without any solvent present. As a result, there is an increasing scientific and industrial interest for the use of aerogels as potential thermal insulators, as matrices for heterogeneous catalysis, in gas storage and gas filtering, in studies of superfluid transitions, and as a refractive medium in Cherenkov detectors (*25, 26*). The fragile solid network of aerogels can possess a density as low as 0.003 g/cm^3 but may still support 1600 times its weight (*27*). The aerogels used for this report (*28*) are alumino-silicate aerogels with densities of 0.1, 0.195, and 0.6 g/cm^3. They can be considered meso-porous, a definition usually assigned to materials with pore sizes between 2 and 50 nm. The diameter of the interconnected alumino-silicate

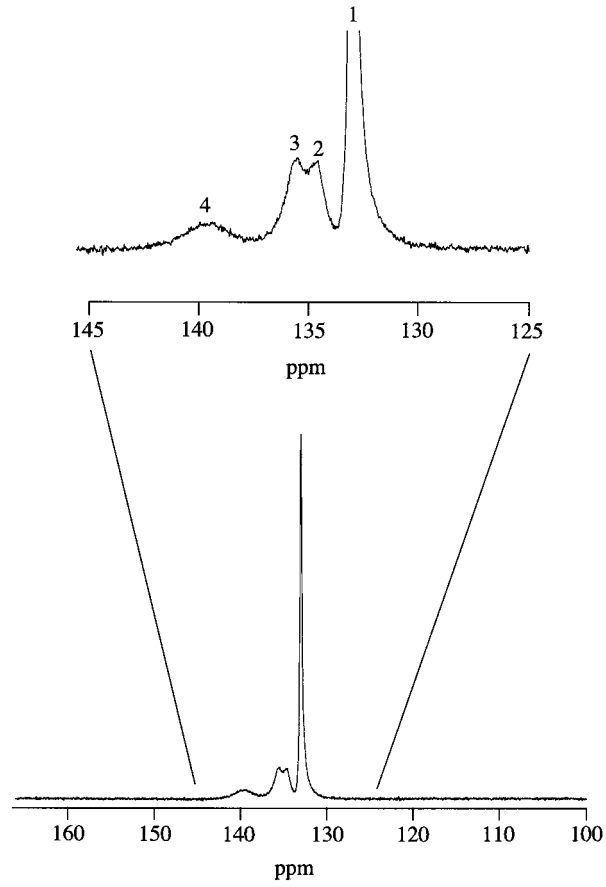

FIG. 2. One dimensional single pulse spectrum of Xenon-131 in a sample of aerogels with three different densities at 283 K. The zoomed plot shows the chemical shift separation between different density aerogels. Identified chemical shift values are: (1) 133 ppm—liquid xenon outside the materials; (2) 134.5 ppm—xenon in 0.1 g/cm^3 aerogel; (3) 135.6 ppm—xenon in 0.195 g/cm^3 aerogel; (4) 139.7 ppm—xenon in 0.6 g/cm^3 aerogel.

particles is typically 1–2 nm, and the aggregation of the particles is fractal until 10–50 nm (*28, 29*).

All experiments were carried out at temperatures around 285 K with natural abundance xenon-131. During sample preparation, the temperature of the xenon may rise above the critical point of 289 K, leading to pressures within the sample tube in excess of 6 MPa. In order to accommodate high pressure we used a sapphire tube as introduced by Roe (*30*) and a valve system similar to the one developed by Horváth and Ponce (*31*) or Merbach and co-workers (*32*). We also added a small inlet screw inside the valve to permit the transfer of bulk material (Fig. 1). After the 10 mm o.d. (outer diameter) sapphire tube was filled with the material of choice, the whole system was connected to a stainless steel transfer line as it was being filled at room temperature with the supercritical natural abundance xenon. For the experiments, the sample was cooled to 283 K, leading to a condensed liquid xenon phase. The longitudinal relaxation time of the pure liquid phase is around $T_1 \approx 110$ ms under these conditions and the density of the xenon is high enough to provide a signal to noise ratio of $S/N \approx 150$ from the 1.8 cm^3 sample after a single scan. Direct shimming on the xenon-131 signal is therefore straightforward but was limited to 8–10 Hz (half-height width of the liquid xenon signal) within the 9.5 mm i.d. sample tube. This procedure proved to be completely sufficient for the experiment since the signal width obtained from xenon inside the cavities of the various aerogels is around 40–115 Hz. No lock channel was used during the experiment since the drift of the magnetic field was much smaller than the signal shift due to temperature fluctuations. The chemical shift of xenon changes by ca. 0.2 ppm per 0.1 K temperature alteration at 283 K, and very stable temperature control is essential for the experiments.

Although the setup should hold pressures around 50 MPa, which provides a sufficient safety margin, it cannot be stressed enough that laboratory personnel should never be exposed directly to the pressurized tube since sapphire tubes may shatter unexpectedly. Workers should be aware that a small temperature increase under conditions close to the critical point may result in a strong pressure increase.

RESULTS

Three dimensional xenon-131 images were acquired with the use of a spin echo pulse sequence. Suppression of the otherwise dominant signal arising from the liquid xenon outside the aerogel is achieved by saturating this transition with a selective sinc-shaped pulse of 22 ms length at the beginning of each experiment. In order to compensate for imperfection of its selectivity, the saturation pulse was followed by a relaxation delay of 12 ms, allowing the xenon-131 inside the aerogel (with its much shorter T_1 relaxation times) to relax partially toward equilibrium. Subsequently, an echo signal was created by a sinc-shaped $\pi/2$ pulse and a π pulse. The echo time was varied in order to produce magnitude images that are weighted

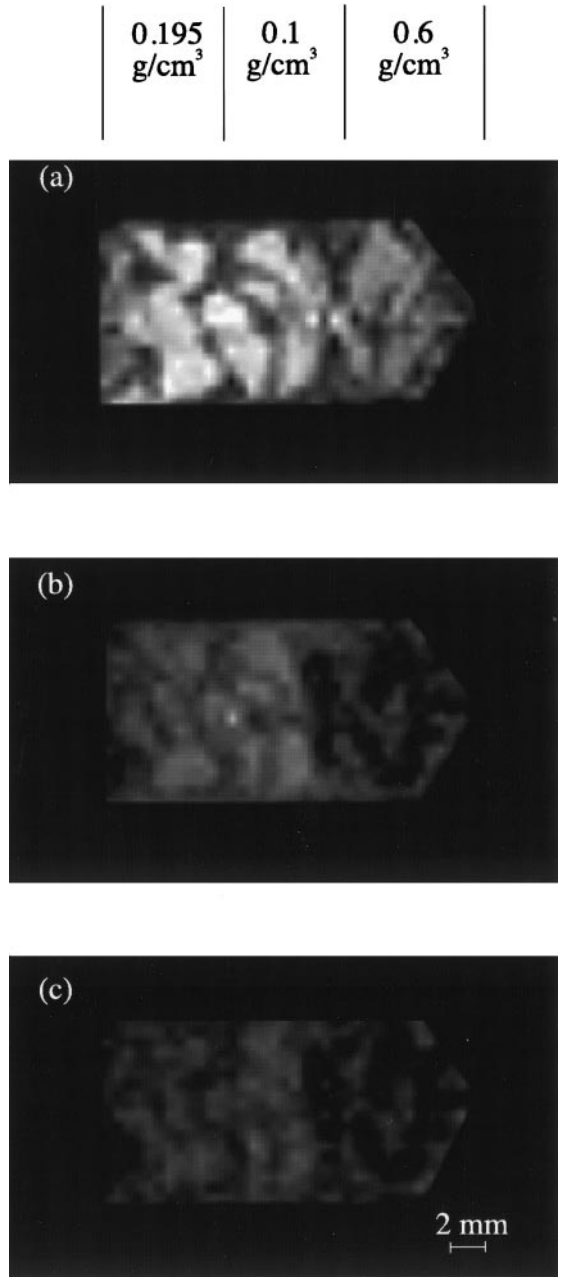

FIG. 3. Relaxation weighed Xenon-131 images of aerogel fragments (1–5 mm diameter) with three densities as a function of echo time (*TE*): (a) $TE = 3.6$ ms, (b) $TE = 8$ ms, (c) $TE = 12$ ms. For short echo times ($TE = 3.6$ ms) the signal arising from the xenon within the aerogel samples appears with slightly different intensities over the background depending on the density of the aerogel host structure. The background intensity which arises from the liquid "void space" xenon surrounding the aerogel fragments has been reduced by T_1 weighting (see Experimental) and is largely independent of the echo-time *TE* due to its small transverse relaxation rate. As the echo time increases, the signals decrease differently due to different relaxation times of the samples. For $TE = 8$ ms the signal from the highest density aerogel has already decayed below the background intensity whereas the signals from the low density fragments appear still brighter than the background. The sapphire tube axis is horizontally oriented in all depicted images.

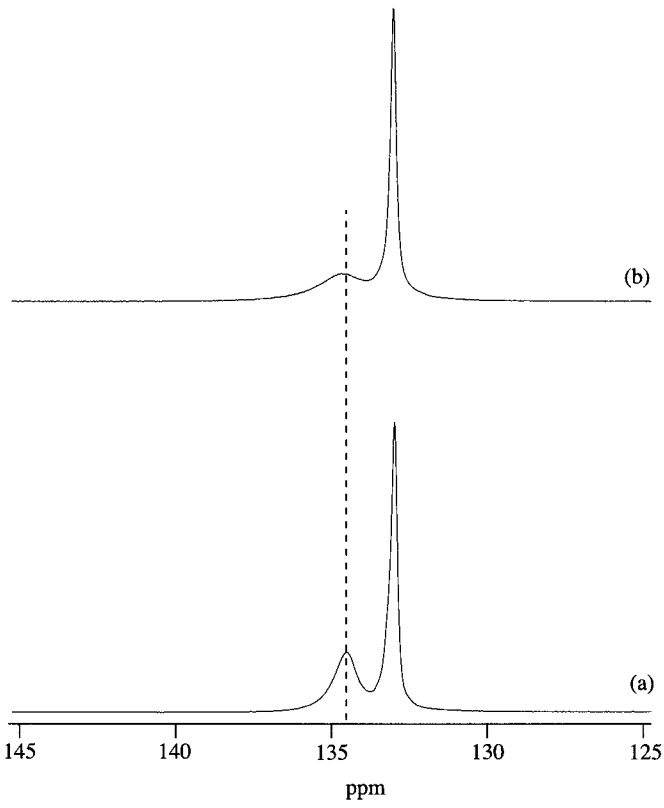

FIG. 4. One dimensional, single pulse spectra of xenon-131 in a sample of an 0.1 g/cm^3 aerogel at 283 K. (a) Untreated 0.1 g/cm^3 aerogel, (b) Aerogel (0.1 g/cm^3) with water removed from the surface. The dashed line shows the slight chemical shift difference of the aerogel peak in these two samples. Note the significant broadening of an aerogel peak in the dried sample (b).

by the quadrupolar interactions of the xenon in the vicinity of the aerogel surface. Images were acquired in 128:32:32 matrices, such that the total number of scans, 245,760, for a single image acquisition took approximately 3 h of experimental time. The matrices were interpolated to 256:64:64 to produce magnitude images with increased digital resolution. The dimensions of a non-interpolated voxel are 0.47 mm in the axis parallel to the static magnetic field (along the sapphire tube axis) and 0.38 $\times$ 0.38 mm in the transverse plane.

Xenon-131 spectra of liquid xenon in aerogels are shown in Fig. 2. The "void space" liquid xenon (i.e., xenon outside the aerogels) displays a chemical shift of 133 ppm, where 0 ppm refers to the predicted shift of xenon gas at 273 K and zero pressure. The aerogel with the highest density (0.6 g/cm^3) shows the largest down field shift (139.7 ppm). Its smaller cavity sizes cause xenon-surface interactions to be more pronounced compared to those of the materials with lower density where xenon has a chemical shift of 135.6 ppm (0.195 g/cm^3) and 134.5 ppm (0.1 g/cm^3). The linewidth also decreases with decreasing density. A half-height width of 115 Hz is observed for the 0.6 g/cm^3 aerogel, 56 Hz for the 0.195 g/cm^3, and 43 Hz for the 0.1 g/cm^3 aerogels, indicating a more pronounced surface contact of the xenon in the higher density materials compared to those with lower density. More surface contact will lead to an increase of transverse quadrupolar relaxation and may also cause a faster dephasing due to coherent quadrupolar evolution if the samples show macroscopic anisotropy. The dephasing due to coherent evolution can in principle be measured by a multiple-quantum filtered experiment (*13*) but we shall restrict the discussion to quadrupolar relaxation for the course of this contribution. A simple measure for the pure relaxational contribution is yielded by the longitudinal relaxation obtained by an inversion–recovery measurement where coherent evolution cannot interfere. The values are $T_1 = 5.3$ ms (0.6 g/cm^3), $T_1 = 8.9$ ms (0.195 g/cm^3), and $T_1 = 11.2$ ms (0.1 g/cm^3), respectively. Therefore, there are at least two possible mechanisms by which to distinguish xenon in different aerogels. One would make use of the chemical shift difference by utilizing selective pulses. The xenon-129 isotope would be the best choice for this kind of experiment due to the larger (absolute) chemical shift separation with larger magnetogyric ratio. The second technique would use the difference in relaxation times in order to produce contrast. We have not attempted T_1 relaxation weighted imaging at this point, although it could be used in principle to obtain the desired contrast between the different surfaces. For simplicity, a spin-echo sequence was chosen in order to avoid any interference with the signal suppression from the "void space" liquid xenon outside the aerogel. The T_1 relaxation times provide a good indication for the possible imaging contrast in this experiment since all measurements indicate a close relationship between the T_1 relaxation and the dephasing in a spin-echo experiment for various surfaces. This dephasing is a result of transverse quadrupolar relaxation and possible quadrupolar evolution of the xenon within the aerogel cavities (*13*). The assignment of T_2 values would be questionable since it is defined only for monoexponential pure relaxation processes. (Indeed, even the T_1 values must be handled with some care, since quadrupolar relaxation of a spin $\frac{3}{2}$ nucleus may be biexponential in some cases (*33*).) The results of the transverse dephasing weighted xenon-131 images for three different echo times are shown in Fig. 3. Clear contrast is obtained between the highest density aerogel and the aerogels of lower density by comparing the images for various echo times, while the contrast between the two low density materials is much less pronounced.

The strength of xenon-131 images weighted by the dephasing of the spin echo due to quadrupolar interactions becomes apparent when the difference in chemical shift is too small for the application of selective pulses. An example is shown in Fig. 4, which displays the spectra of xenon-131 in aerogel fragments of 0.1 g/cm^3 density. Figure 4b shows the spectrum where the surface water has been removed from the aerogel, whereas no special treatment has been applied to the aerogel for the spectrum in Fig. 4a, which is identical to the corresponding transition of the spectrum in Fig 2. In order to remove the surface adsorbed water, the material was heated for half an

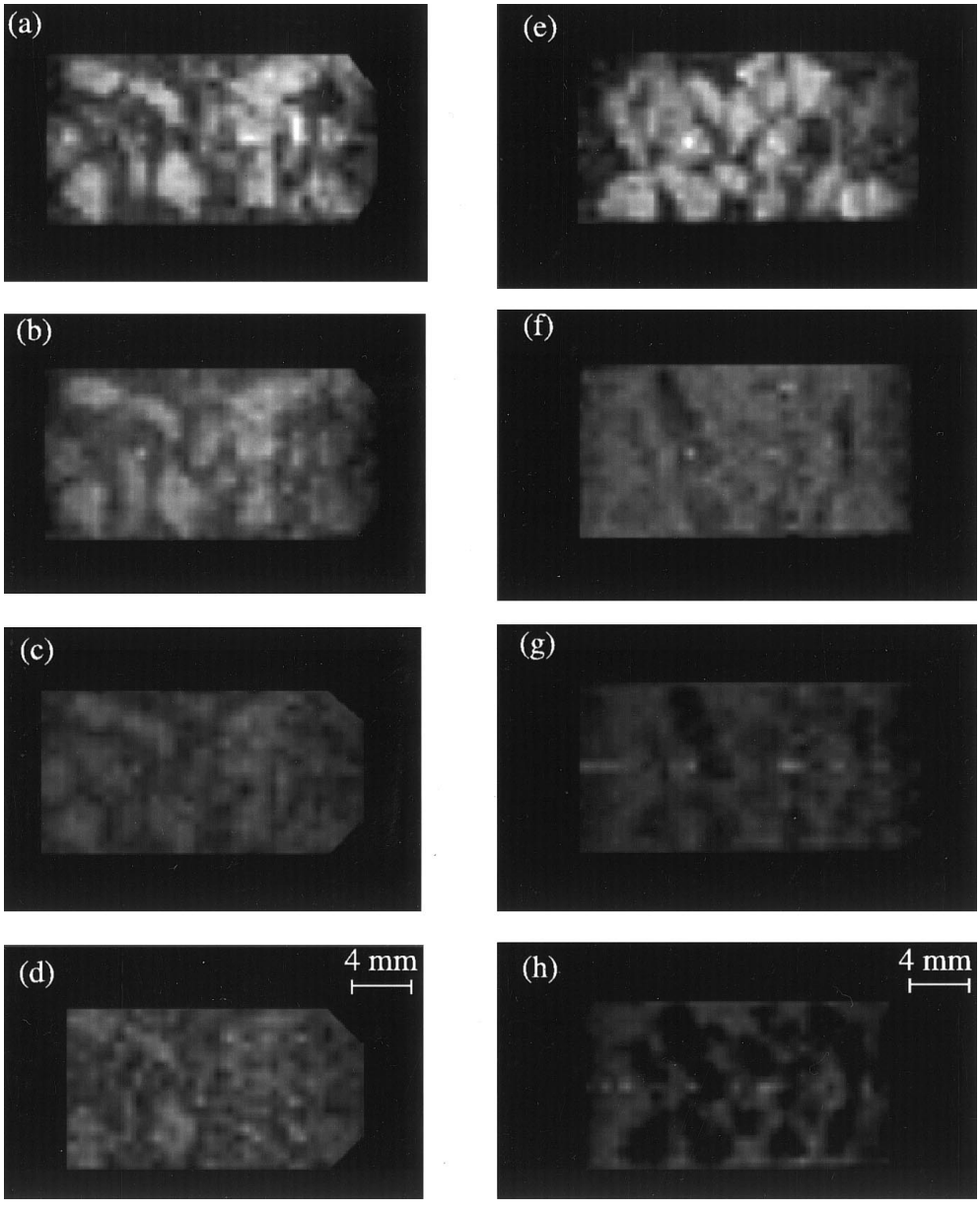

FIG. 5. (a–d) Relaxation weighed Xenon-131 images of untreated 0.1 g/cm^3 aerogel pieces as a function of echo time (*TE*): (a) $TE = 3.6$ ms, (b) $TE = 7$ ms, (c) $TE = 9$ ms, (d) $TE = 12$ ms. (e–h) Relaxation weighed Xenon-131 images of 0.1 g/cm^3 aerogel with water removed from the surface as a function of echo time (*TE*): (e) $TE = 3.6$ ms, (f) $TE = 7$ ms, (g) $TE = 9$ ms, (h) $TE = 12$ ms. For short echo times ($TE = 3.6$ ms) both aerogel samples appear brighter as the background (see also the caption of Fig. 3). For larger echo times, the signal from the degassed sample decreases rapidly and cannot be distinguished from the background at $TE = 7$ ms (f). It appears as "dark" fragments at $TE = 9$ ms (g), where the corresponding signal from the non-treated sample is still above the background intensity (c).

hour to an estimated 400 K in vacuum until the final pressure of about 10 Pa had been reached. The transition of the xenon-131 inside the treated aerogel has a chemical shift of 134.7 ppm, which is about 0.2 ppm different from that of the non-degassed sample. This makes selective experiments very dubious, since lineshape overlap must be expected even in a xenon-129 spectrum. However, the relaxation times are substantially different, with $T_1 = 11.2$ ms for the untreated and $T_1 = 3.6$ ms for the treated host structure. An explanation for this phenomenon is that a portion of the surface bound water is removed by the heating (the effect is reversible) and the degassed surface sites may be more lipophilic—i.e., the xenon will have a longer residence time on this particular site than on the polar surface sites already occupied by water molecules. Therefore, xenon-131 can be employed as a surface probe, as shown in Fig. 5. (i.e., Figs. 5a–d, non-degassed; Figs. 5e–h, degassed).

Recently (*15*), a dispersion of the transverse relaxation times of xenon-129 for different aerogels was reported. One possible explanation is a change of the average local susceptibility with changing density. This is in contrast to the xenon-131 relaxation, which depends directly on surface interactions and can therefore probe surface coatings. For this study we examined the transverse relaxation of xenon-129 within the 0.1 g/cm^3 aerogel, using 150 kPa of xenon with approximately 3 kPa of added oxygen as a relaxation agent. No change in the transverse relaxation behavior was noticeable for the degassed versus non-degassed material with $T_2 = 35$ ms for both cases.

Xenon with natural abundance (21.18% of ^{131}Xe) has been used for all experiments described in this contribution. Enriched ^{131}Xe (80% and 99%) is commercially available and its usage would lead to a substantial S/N enhancement even at lower fields. The very high cost could be reduced if the design of the experimental setup were modified to limit the amount of xenon used for the experiment. Xenon can easily be recycled due to its high freezing point (161.3 K at atmospheric pressure).

While the signal intensity of ^{131}Xe is comparable to the intensity of ^{129}Xe in these materials due to the much faster repetition time, it is orders of magnitude weaker than those obtained from optical pumped ^{129}Xe experiments or experiments using protonated solvents. The benefit of ^{131}Xe is that the contrast of the images can be attributed to the quadrupolar interaction on the surface of porous materials. The setup described has the additional advantage that the transfer of xenon can be accomplished under supercritical conditions without destroying or altering the test materials (such as the fragile aerogels) inside the tube.

CONCLUSION

This report shows the first examples of successful xenon-131 images. It also shows the potential value of this isotope as a surface sensitive contrast agent. Future applications are not restricted to different levels of hydration of the surface, but they might also include surface coatings or grafting, surface geometry and the surfaces of catalysts like solid superacids such as sulfonated metal oxides. Xenon-131 imaging might be of particular importance in characterizing the homogeneity of the macroscopic distribution on hydrophobic grafting on amorphous materials.

An important limitation of this technique is its restriction to non-paramagnetic materials since paramagnetic relaxation can easily dominate over quadrupolar interactions. In the case of paramagnetic impurities, xenon-129 or protonated liquids may provide a larger range of relaxation rates and therefore a stronger contrast for imaging.

Xenon-129 spectroscopy has been very useful in the study of materials where the chemical shift of the xenon can be exploited as a probe for micro-porous host structures. Quadrupolar relaxation of the xenon-131 isotope can serve as an additional, very sensitive probe that may provide valuable complementary information for the study of solid/gas (solid/liquid) matrices. Current research also concerns coherent quadrupolar evolution on the surface (*13*), which may provide information about order parameters in materials. Xenon-131 MRI will be of particular importance for materials with comparably large cavities—i.e., meso-porous structures, where the chemical shift may be a less sensitive probe for the surface properties.

ACKNOWLEDGMENTS

This work was performed at the National High Magnetic Field Laboratory supported by the National Science Foundation Cooperative Agreement DMR-9527035 and the State of Florida.

REFERENCES

1. A. K. Jameson, C. J. Jameson, and H. S. Gutowsky, *J. Chem. Phys.* **53,** 2310–2320 (1970).
2. T. Ito and J. Fraissard, *in* "Proceedings, Fifth International Conference on Zeolites" (L. V. C. Rees, Ed.), p. 510, Heyden, London/Naples (1980).
3. J. A. Ripmeester, *in* "Presented at the ISMAR–Ampère International Conference on Magnetic Resonance, Delft, The Netherlands, 1980."
4. J. A. Ripmeester, *Bull. Magn. Reson.* **79,** 139–140 (1981).
5. J. A. Ripmeester and D. W. Davidson, *J. Mol. Struct.* **75,** 67–68 (1981).
6. T. Ito and J. Fraissard, *J. Chem. Phys.* **76,** 5225–5229 (1982).
7. D. Raftery and B. F. Chmelka, *NMR Basic Principles and Progress* **30,** 111–158 (1994).
8. C. I. Ratcliffe, *Annu. Rep. NMR Spectrosc.* **30,** 111–158 (1998).
9. A. Loewenstein and M. Brenman, *Chem. Phys. Lett.* **58,** 435–436 (1978).
10. P. Diehl and J. Jokisaari, *J. Magn. Reson.* **88,** 660–665 (1990).
11. P. Ingman, J. Jokisaari, and P. Diehl, *J. Magn. Reson.* **92,** 163–169 (1991).
12. J. Jokisaari, *Progr. NMR Spectrocs.* **26,** 1–26 (1994).
13. T. Meersmann, S. A. Smith and G. Bodenhausen, *Phys. Rev. Lett.* **80,** 1398–1401 (1998).
14. T. Meersmann and M. Haake, *Phys. Rev. Lett.* **81,** 1211–1214 (1998).
15. D. M. Gregory, R. E. Gerald, and R. E. Botto, *J. Magn. Reson.* **131,** 327–335 (1998).
16. D. M. Gregory *et al., in* "Spacially Resolved Magnetic Resonance: Methods, Materials, Medicine, Biology, Diffusion, Flow, Geology, Ecology, Hardware" (P. Blümler, B. Blümlich, and R. E. Botto, Eds.), Wiley–VCH, New York, 1998.
17. M. S. Albert, G. D. Cates, B. Dreihuys, W. Happer, B. Saam, C. S. J. Springer, and A. Wishnia, *Nature* **370,** 199–201 (1994).
18. H. Middlleton, R. D. Black, B. Saam, G. D. Cates, G. P. Cofer, R. Guenther, W. Happer, L. W. Hedlund, G. A. Johnson, M. D. Shattuck, and J. C. Schwartz, *Magn. Reson. Med.* **33,** 271–275 (1995).
19. M. Leduc and E. Otten, *La Rechèrche* **287,** 41–43 (1996).
20. B. M. Goodson, Y.-Q. Song, R. E. Taylor, V. D. Schepkin, K. M. Brenman, G. C. Chingas, T. F. Budinger, G. Navon, and A. Pines, *Proc. Natl. Acad. Sci. U.S.A.* **94,** 14725–14729 (1997).

21. D. Raftery, H. Long, T. Meersmann, P. J. Grandinetti, L. Reven, and A. Pines, *Phys. Rev. Lett.* **66,** 584–587 (1991).
22. S. S. Kistler, *Nature* **127,** 741 (1931).
23. J. Fricke and A. Emmerling, *J. Am. Ceram. Soc.* **75,** 2027–2036 (1992).
24. L. W. Hrubesh and R. W. Pekala, *J. Non-Cryst. Solids* **188,** 46–53 (1995).
25. P. A. Crowell, G. K. S. Wong, and J. D. Reppey, *Physica B* **1165,** 614–617 (1990).
26. P. Carlson, *Nucl. Instrum. Methods Phys. Res. Sect. A* **248,** 110–117 (1986).
27. L. W. Hrubesh, *Chem. Ind.* 824–827 (1990).
28. F. Chaput, J.-P. Boilot, A. Dauger, F. Devreux, and A. D. Geyer, *J. Non-Cryst. Solids* **116,** 133–139 (1990).
29. H. D. Gesser and P. C. Goswami, *Chem. Rev.* **89,** 765–788 (1989).
30. D. C. Roe, *J. Magn. Reson.* **63,** 388–391 (1985).
31. I. T. Horvath and E. C. Ponce, *Rev. Sci. Instrum.* **62,** 1104–1105 (1991).
32. A. Cusanelli, U. Frey, D. T. Richens, and A. E. Merbach, *J. Am. Chem. Soc.* **118,** 5265–5271 (1996).
33. G. Jaccard, S. Wimperis, and G. Bodenhausen, *J. Chem. Phys.* **85,** 6282–6293 (1986).